BNL-NUREG-33696

CONF-8310205--1

STRESS CORROSION OF ASTM GRADE-2 AND GRADE-12 TITANIUM IN SIMULATED ROCK SALT BRINES AT 83°C*

H. Jain, T. M. Ahn and P. Soo
Department of Nuclear Energy
Brookhaven National Laboratory
Upton, New York 11973
USA

BNL-NUREG--33696

DE84 001212

Slow-strain-rate tests have been conducted on Grade-2 and Grade-12 titanium in simulated rock salt brines at 83°C. Although neither metal shows stress corrosion cracking, total elongation and reduction in area show some decrease. Optical and SEM results are discussed to elucidate the fracture mechanism.

*This work was performed under the auspices of the U. S. Nuclear Regulatory Commission.

EMP

Introduction

Due to its very high general corrosion resistance in brine, ASTM Grade-12 titanium alloy (nominally containing 0.3% Mo and 0.8% Ni by weight) is a candidate container material for the disposal of high level nuclear waste in a salt repository in the U.S.A. In the past, many of the titanium alloys have shown high susceptibility to hydrogen embrittlement (1,2) and stress corrosion cracking in chloride containing environments (2,4). In a salt repository, the waste container is likely to be subjected to both of these interrelated phenomena, and, therefore, it is important to characterize the mechanical behavior of Grade-12 titanium under simulated repository conditions.

To examine the environmentally assisted degradation of an alloy, its mechanical properties are measured in the test solution and compared with those in an inert environment. Mechanical property changes are usually more noticeable the slower the strain rate. Accordingly, we have studied Grade-12 titanium in various brine solutions and measured its ultimate tensile strength (UTS), total elongation and reduction in area (RA) using a slow-strain-rate testing machine. The experiments at Sandia National Laboratory (5,6) carried out under somewhat similar conditions have not shown any large mechanical degradation, although some loss in ductility near the specimen surface was reported to be due to reactions with the brine solution. To understand the origin of such near surface changes in the failure mode, as well as the role of alloying elements in Grade-12 titanium, parallel tests were conducted on commercially pure titanium. Since highly acidic conditions (e.g. in a crevice) or alkaline conditions [due to the formation of colloidal sodium in rock salt during gamma irradiation (7)] might develop in a salt repository, these two materials were tested in brine solutions with pH ranging from 1 to 11.

Experimental

Most of the slow-strain-rate tests were performed on 1.27-cm diameter Grade-12 or 0.635-cm diameter Grade-2 commercially pure (C.P.) titanium rods. The chemical analyses of these materials as supplied by the vendor are given in Table I. The microstructure of the Grade-12 alloy shows a strong texture along the axis of the rod (Figure 1), whereas C.P. titanium rods have an equiaxed grain distribution (Figure 2).

Table I. Chemical Composition of Grade-2 and Grade-12 Titanium (Weight Percent)

	C	N	H	Fe	O	Mo	Ni	Ti
Grade-2	0.04	0.018	0.0041	0.11	0.152	---	---	balance
Grade-12	0.011	0.011	0.0046	0.06	0.150	0.28	0.73	balance

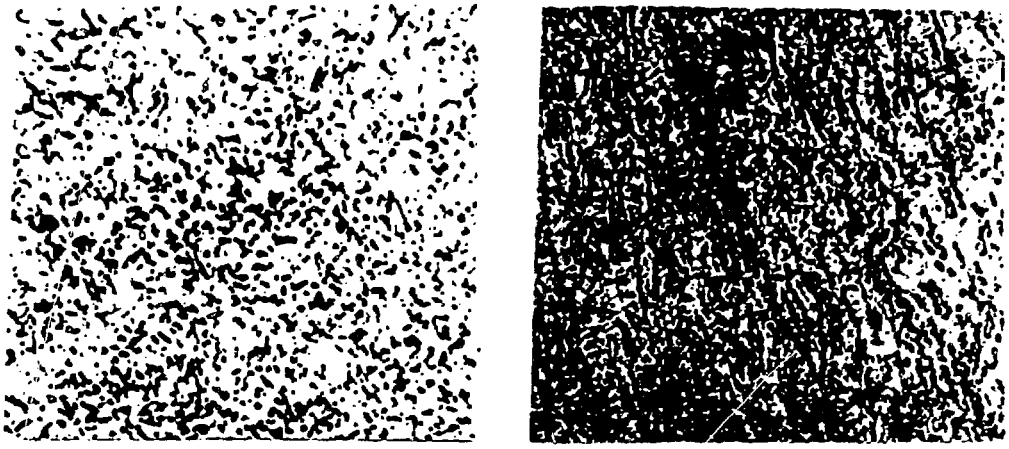

(a) (b)

Figure 1 - Microstructure of Grade-12 titanium rod. (a) Cross section perpendicular to the axis of the rod, (b) cross section parallel to the axis of the rod. X1000.

Figure 2 - Microstructure of Grade-2 titanium rod. This structure shows equiaxed grains. Acicular transformed alpha phase is found across the grains, particularly near the surface. X400.

Smooth tensile test specimens were prepared by machining 0.635-cm threads on both ends of a 22.9-cm long piece of rod with a 1.27-cm long and 0.254-cm diameter gauge in the center. Specimens were deformed in tension at a constant strain rate which was maintained by a gear reducer assembly and a motor. An approximately 15-cm long central portion of each specimen was enclosed in a Teflon cylinder which contained the required test environment at a given temperature. In some cases, the corrosion potential of the specimen was monitored using a potentiostat (EG G Model 363). After a test, the fractured surface of each specimen was examined using optical and scanning electron microscopes.

To investigate the effects of externally introduced hydrogen, a few Grade-12 unnotched sheet specimens (gauge length = 2.54 cm and thickness = 0.9 mm) were machined according to ASTM specifications (8) and tested in air at room temperature using an Instron tensile testing machine. These were hydrogenated cathodically in 10% sulfuric acid with 3.1×10^{-3} M $Na_4P_2O_7$ cathodic poison for one-half to one hour at 90°C and 15 mA/cm^2.

The chemical compositions of the two synthetic brines (A and B) used in the present study, which are considered to be representative of the brines in Carlsbad (New Mexico) salt are given in Table II. To make Brine A acidic and Brine B alkaline, HCl and NaOH, respectively, were added until the desired pH was achieved.

Table II. Compositions of Brine Solutions

Component	Concentration (ppm) Brine A	Brine B
Na^+	42,000	115,000
K^+	30,000	15
Mg^{+2}	35,000	10
Ca^{+2}	600	900
Sr^{+2}	5	15
Cl^-	190,000	175,000
SO_4^{-2}	3,500	3,500
I^-	10	10
HCO_3^{-1}	700	10
Br^-	400	400
BO_3	1,200	10

Results

Mechanical Properties

Typical stress-strain as well as corrosion potential versus nominal strain curves for Grade-12 and C.P. titanium are shown in Figure 3. Ultimate tensile strength and total elongation are determined from such curves for both alloys. The reduction in area is measured from SEM photographs of the fracture surface. The results obtained on cylindrical specimens are listed in Table III for different test environments. All the specimens were deformed at a nominal strain rate of 3.0×10^{-7}/sec, except for Tests 6 and 7 where a faster rate of 1.5×10^{-6}/sec was used. The results of tensile tests on sheet specimens in as-received and after hydrogenation are listed in Table IV. These tests were performed under ambient conditions and at nominal strain rates of 1.2×10^{-2}/sec or 2.5×10^{-5}/sec. The difference between the two sets of data of room temperature mechanical properties shown in Tables III and IV could be primarily due to the difference in strain rates, or size and texture of the grain structure.

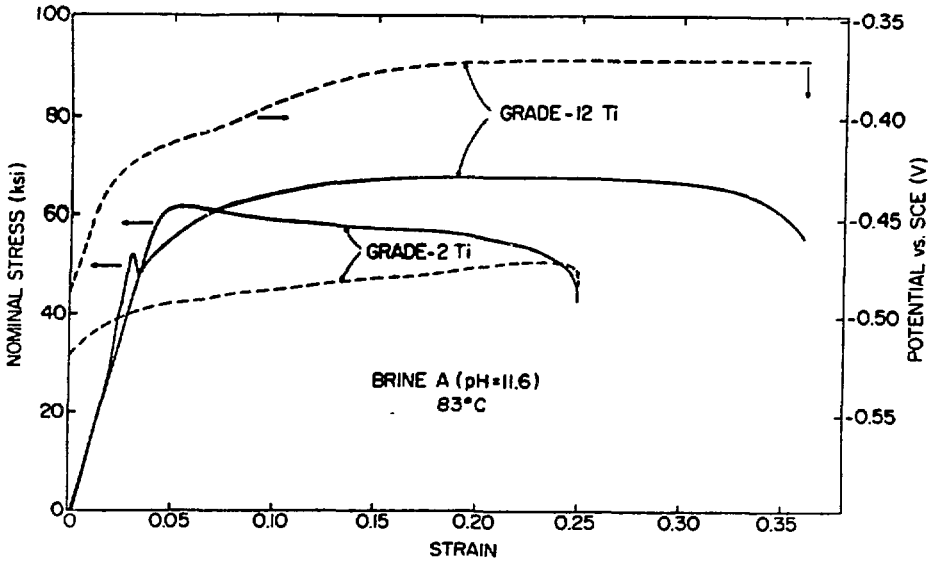

Figure 3 - Typical engineering stress vs strain curves for Grade-2 and Grade-12 titanium specimens (solid line). Variation of simultaneously measured potential of both the specimens is shown by the broken lines.

Table III. Slow-Strain-Rate Test Results for Grade-2 and Grade-12 Titanium.[a]

Test No.	Material	Environment	Temp. (oC)	Maximum Stress (ksi)	Total Elongation, e (%)	R.A. (%)
1	CP Ti	Air	R.T.	77.1	19.5	48.6
13	CP Ti	He	84.1	58.1	20.5	51.9
20	CP Ti	Air	82.9	59.3	19.8	50.9
11	CP Ti	Deionized Water	83.5	55.9	17.9	47.7
15	CP Ti	Brine A	83.1	56.6	19.2	44.0
8	CP Ti	Acidic Brine A[b]	84.8	59.5	18.8	46.4
5	CP Ti	Alkaline Brine B[c]	83.2	60.0	20.0	44.0
6	CP Ti	Alkaline Brine B[c]	84.6	63.8	24.2	45.9
3	TiCode-12	Air	R.T.	74.8	25.3	47.6
14	TiCode-12	He	83.7	68.7	36.6	51.5
19	TiCode-12	Air	82.5	70.0	33.8	49.2
12	TiCode-12	Deionized Water	83.1	65.7	--	52.9
18	TiCode-12	Brine A	82.2	64.8	31.6	50.3
10	TiCode-12	Acidic Brine A[b]	83.7	64.9	--	52.0
4	TiCode-12	Alkaline Brine B[c]	82.0	63.4	32.0	52.0
7	TiCode-12	Alkaline Brine B[c]	82.3	67.8	36.8	53.2

[a]Strain rate $\dot{e} = 3.0 \times 10^{-7}$/sec, except for the test numbers 6 and 7, where $\dot{e} = 1.5 \times 10^{-6}$/sec.

[b]Acidic Brine A was prepared by adding HCl until the pH of the solution reached 1.0.

[c]Alkaline Brine B was prepared by adding NaOH until the pH of the solution reached 11.6.

Table IV. Tensile Test Results for As-Recived and Hydrogenated Grade-12 Titanium Sheet Specimens at Room Temperature

Strain Rate	1.2×10^{-2}/sec		2.5×10^{-5}/sec	
	UTS (ksi)	Total Elongation (%)	UTS (ksi)	Total Elongation (%)
As-received	99.9	22	91.7	31
Hydrogenated	98.5	22	88.9	20

Fractographs

Representative SEM micrographs taken normal to the macroscopic fracture surfaces of Grade-12 and C.P. titanium are shown in Figures 4 and 5, respectively. Note that in the case of Grade-12 specimens, the edge has a different appearance from the central zone. Within the variation along the periphery, the width of this edge region was nearly independent of the test environment or the strain rate used. For C.P. titanium, the equivalent edge region is negligibly small.

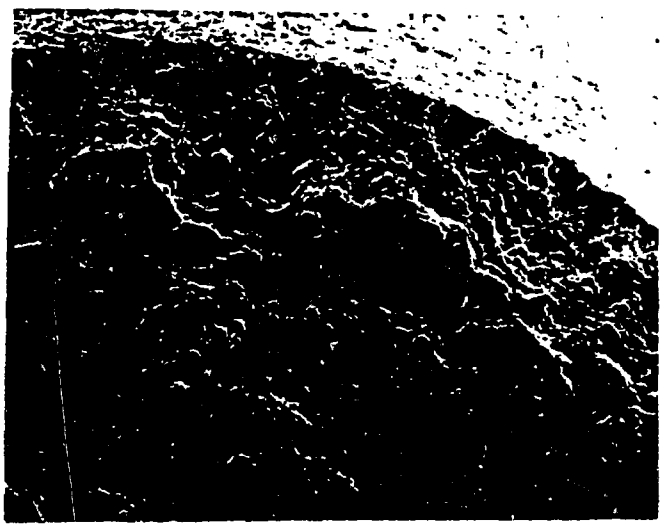

Figure 4 - A typical SEM fractograph of a Grade-12 titanium specimen. Note the quasi cleavage type feature near the edge (top part of the picture). X200.

A magnified view of an edge region is shown in Figure 6; the two micrographs represent mating regions on the two halves of a fractured specimen. Note that the rounded ends of dimples on the two halves point in opposite directions. An examination of the Grade-12 fracture surface under an optical microscope shows that the distinctive edge region is at an angle with the macroscopic fracture plane (which is normal to the tensile axis). A view of the edge region roughly normal to the incident electron beam is obtained (Figure 7) after tilting the specimen by 45°.

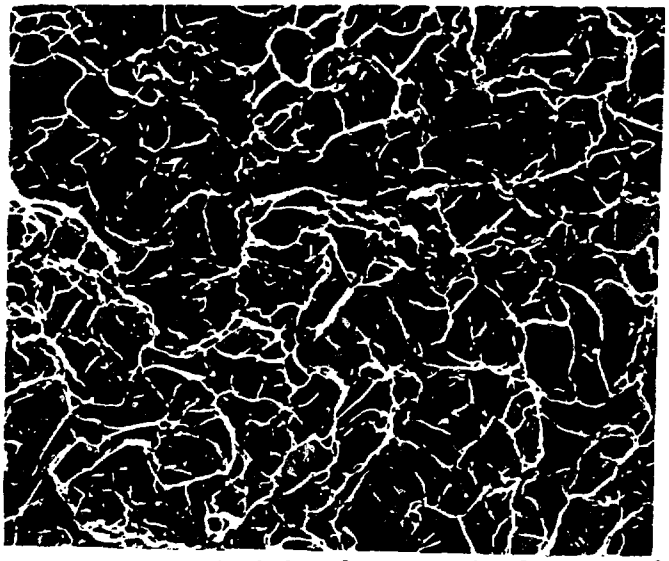

Figure 5 - A typical SEM fractograph of a Grade-2 titanium specimen. X200.

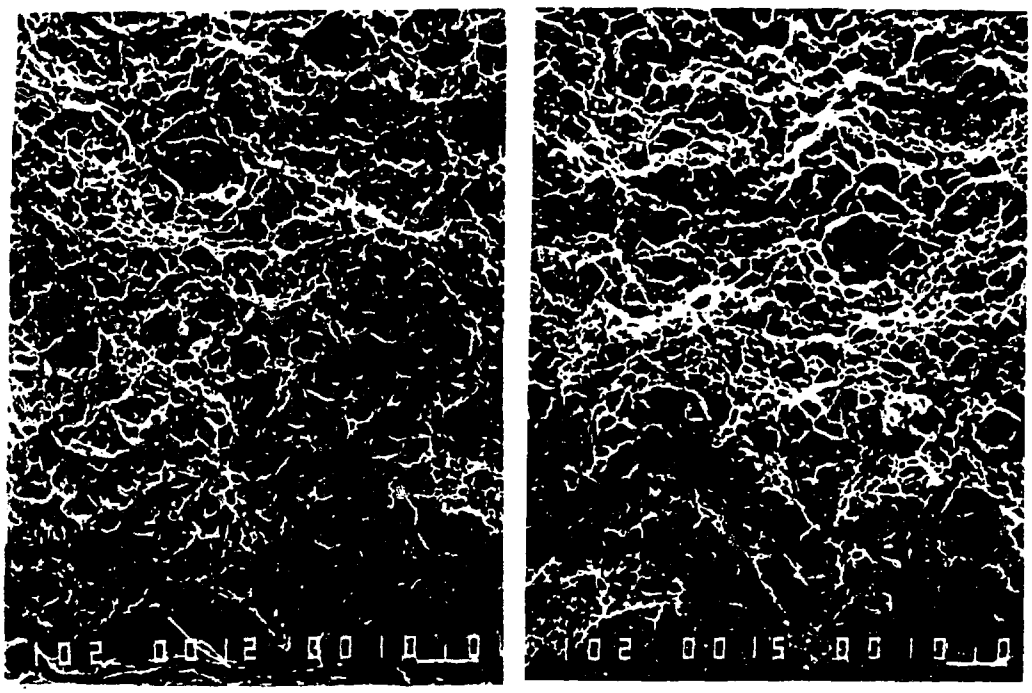

(a) (b)

Figure 6 - SEM photographs of the mating regions of a fractured Grade-12 titanium specimen; (a) is the cone and (b) is the cup half. X1000.

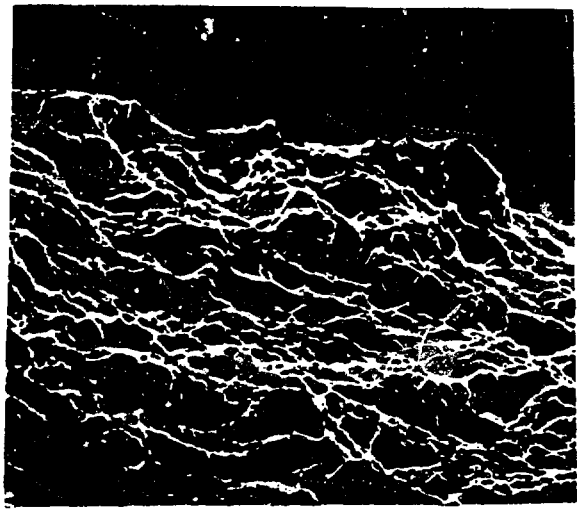

Figure 7 - A SEM photograph of the edge region of a Grade-12 titanium specimen tilted by 45° to bring the edge region normal to the electron beam. X1000.

To understand the large difference between total elongation of the two metals, the longitudinal sections of the fractured specimens were examined. Note the difference in the size and distribution of voids below the fracture surface of C.P. and Grade-12 titanium as shown in Figures 8 and 9, respectively.

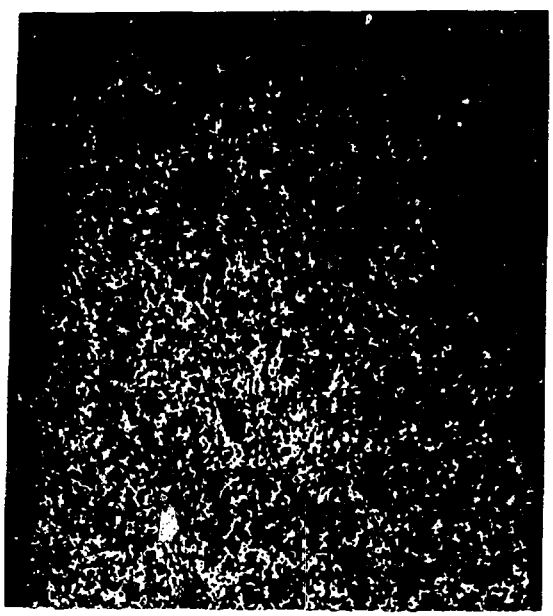

Figure 8 - A longitudinal section of a Grade-2 titanium specimen showing a relatively small number of large voids below the fracture surface. The voids appeared to have nucleated at grain boundary triple points, and then grew across the grains. X50.

Figure 9 - A longitudinal section of a Grade-12 titanium specimen showing numerous small voids below the fracture surface. X150.

Discussion

The results described in Table III for C.P. and Grade-12 titanium indicate that, in general, the latter alloy has superior mechanical properties. For either of the materials an increase in strain rate increases the values of UTS, RA and total elongation. A similar strain rate dependence was observed by Abrego and Rack (5) and Pitman (9).

Figure 3 and Table III describe some interesting differences between the two metals. Grade-12 titanium shows a well defined yield point indicative of strain aging effects. C.P. titanium starts necking at a very early stage, and does not show a sharp yield point which has been noticed earlier under different conditions of strain rate and temperature (10). The reduction in area for the two metals is comparable, but Grade-12 titanium has a much larger value for total elongation. This observation is consistent with the fact that compared to C.P. titanium, the neck in Grade-12 titanium is more shallow. Such differences in the behavior of the two metals can be explained by the presence of the alloying elements and small amounts of beta phase which cause much stronger strain hardening in the alloy. An order of magnitude smaller grain size in the Grade-12 titanium may also contribute to its strain hardening. Because of strong work hardening, the plastic strain in Grade-12 titanium tends to propagate into previously undeformed areas, thus producing many voids of small size (Figure 9) as well as forming a shallow neck. On the other hand, due to low strain hardening in C.P. titanium, a neck that is formed continues to shrink locally due to higher stress intensity. For C.P. titanium, the larger grain size offers fewer nucleation sites for the formation of voids, but once a void is formed it continues to grow easily in a transgranular fashion (Figure 8).

To quantify the environmentally assisted degradation of mechanical properties, air has been usually chosen as the reference atmosphere (5,9). Present results (Table III) show that a helium environment gives better mechanical properties than air and, therefore, should be preferred as a reference. The reason for poorer properties in air is not clear, but this may be the cause of some of the earlier reported apparent improvement in the properties of Grade-12 titanium when tested in brine or seawater (5).

There is no indication of stress corrosion cracking under any of the test conditions used. A monotonic increase in the corrosion potential of a specimen (except at failure) during straining is consistent with the idea that no macroscopic cracks are produced. In other words, any rupture of oxide film during straining is repaired soon enough to allow any observable change in potential due to the exposure of bare metal surface to solution (such as at the time of sample failure). Nevertheless, macroscopic mechanical properties show a definite loss in ductility of Grade-12 titanium in neutral Brine A, and of C.P. titanium in Brine A as well as alkaline Brine B. However, there is no major difference between the fractographs of either metal whether tested in Brine A or in helium. In the case of Grade-12 titanium, the edge of fracture surface has a markedly different appearance than its center (Figures 4 and 6). Abrego and Rack (5) have suggested that this so-called quasi cleavage fracture occurring at a Grade-12 titanium specimen edge is presumably due to attack from the corrosion environment. To examine this hypothesis and to further understand this near edge behavior in Grade-12 titanium, we note that:

(a) The so-called "quasi cleavage" fracture mode is always seen near the specimen edge. It constitutes the shear lip zone of the cup and cone halves of a specimen, where the fracture plane is at an angle with respect to central area. Such observations are expected for a ductile fracture which is quite evident from the dimples and tear ridges found in the central area. That the fracture at the edge occurs predominantly by shearing is confirmed in Figure 6 where rounded edges of dimples at the mating surfaces point in opposite directions.

(b) The flatness in the edge region (Figures 4 and 6), which gives the impression of a quasi cleavage fracture mode, becomes less clear when the edge is examined in a normal-to-the-edge view (Figure 7).

(c) For the same conditions of temperature and strain rate, the width of the edge region is nearly the same for all the tests, although the mechanical properties differ.

(d) C.P. titanium specimens show similar environmental effects but without any quasi cleavage zone.

(e) Abrego and Rack find that the width of the quasi cleavage zone is increased by immersing a Grade-12 specimen in brine under γ-irradiation conditions (where H_2 is likely to be absorbed on the specimen surface) as well as by heat treating a specimen (where no environmental effect is expected).

These observations suggest that a simple examination of the so-called "quasi cleavage" area of the fracture surface does not reveal any obvious correlation with the kind of environmentally assisted loss in ductility observed in the present experiments. Also, the external effects alone are not responsible for the edge effect. It is possible that this effect is due to very different shear stresses acting on the edge area just before the specimen fails. However, we note that:

(a) At an elongation rate of 2.5×10^{-5}/sec, the edge effect is larger in the hydrogen charged specimen than in the as-received specimen. In the present cathodic charging the hydrogen is concentrated near the surface. Thus, there is a correlation between the presence of hydrogen and the edge effect. Molecke and others have also made similar suggestions (10). In the samples having higher uniform hydrogen concentration, the whole fracture surface may show flat areas of a brittle failure (11,12).

(b) The quasi cleavage appearance near the edge in Figures 4 or 6 is distinct and is not found in the central zone after tilting the specimen by 45°. That is, some of the flatness in the edge region cannot be explained in terms of the viewing angle.

On the basis of the above discussion, it is concluded that the quasi cleavage appearance near the edge of Grade-12 specimens has little correlation with the presence of brine. Most likely it is caused by internal hydrogen (46 ppm in the present alloy) which concentrates by some mechanism near the edge during the test or at the time of initial sample preparation. In this respect we note that stress induced hydrogen embrittlement is well known in titanium alloys (1,13). The quasi cleavage zone and shear lip occur at the specimen edge, but probably the two are not related.

References

1. N. E. Paton and J. C. Williams, "Effect of Hydrogen on Titanium and Its Alloys," in Hydrogen in Metals, I. M. Bernstein and A. W. Thompson, Editors, p. 409, ASM, Ohio, 1974.

2. T. F. Archbold and D. H. Polonis, "Assessment of Delayed Failure Modes in Titanium and Titanium Alloys," PNL-4127, Pacific Northwest Laboratory, Richland, Washington, 1981.

3. Stress Corrosion Cracking of Titanium, STP 397, ASTM, 1966.

4. M. J. Blackburn, J. A. Feeney and T. R. Beck, "Stress Corrosion Cracking of Titanium Alloys," in Advances in Corrosion Science and Technology, Vol. 3, M. G. Fontana and R. W. Staehle, Editors, Plenum Press, New York, 1973.

5. L. Abrego and H. J. Rack, "The Slow Strain Rate Behavior of TiCode-12 in Aqueous Chloride Solutions," Paper No. 97 in Corrosion '81, NACE, April 6-10, 1981, Toronto, Canada.

6. M. A. Molecke, D. W. Schaefer, R. S. Glass and J. A. Ruppen, "Sandia HLW Canister/Overpack Studies Applicable for a Salt Repository," SAND81-1585, Sandia National Laboratory, 1981.

7. S. V. Panno and P. Soo, "An Evaluation of Chemical Conditions Caused by Gamma Irradiation of Natural Rock Salt," Brookhaven National Laboratory Report, to be published.

8. "Standard Methods of Tension Testing of Metallic Materials," ASTM E8-79, Annual Book of ASTM Standards, Part 10, 1979.

9. S. G. Pitman, "Investigation of Environmentally Assisted Fracture of Metallic Nuclear Waste Package Barrier Materials in Simulated Basalt Repository Environments," PNL-4379, Pacific Northwest Laboratory, 1982.

10. F. D. Rosi and F. C. Perkins, "Mechanical Properties and Strain Aging Effects in Titanium," Trans. ASM, 45 (1953) p. 972.

11. M. A. Molecke, J. A. Ruppen and R. B. Diegle, "Materials for High Level Waste Canister/Overpacks in Salt Formations," SAND82-0429, Sandia National Laboratory, 1982.

12. T. M. Ahn and P. Soo, "Internal Hydrogen Embrittlement of Titanium Alloy TiCode-12 at Room Temperature," NUREG/CR-3282, BNL-NUREG-51671, Brookhaven National Laboratory, 1983.

13. N. R. Moody and W. W. Gerberich, "Hydrogen Induced Slow Crack Growth in Ti-6Al-6V-2Sn," Met. Trans., 11A (1980) p. 973.